MRI Image-Based Mapping of Human Head Motion and Brain Ventricular Cerebrospinal Fluid Flows Using Computer Vision

Jin Xu[1], William W. Liou[1(✉)], Shinya Yamada[2,3], Madoka Nakajima[2], Masakazu Miyajima[2], and Ko Horikoshi[2]

[1] Western Michigan University, Kalamazoo, MI 49008, USA
william.liou@wmich.edu
[2] Department of Neurosurgery, Juntendo University, Tokyo, Japan
[3] Department of Neurosurgery, Kugayama Hospital, Tokyo, Japan

Abstract. Cerebrospinal fluid (CSF) plays a critical role in brain metabolism and protection from external forces. Traditional MRI can provide some insights into CSF dynamics; however, more advanced and cost-effective methods are needed for precise and comprehensive visualization of flow patterns, velocities, and directions in clinical settings. In this paper, we demonstrate a new application of a few open-source computer vision software packages to capture CSF motion from time spatial inversion pulse (Time-SLIP) MRI clinical images (in DICOM format). To test the hypothesis that the CSF flow depends on head motions, a reliable and robust pipeline of processing Time-SLIP MRI images is developed to extract both anatomy and CSF motion dynamics. The paper presents a methodology for extracting unsteady flow information from Time-SLIP MRI images and the results of its application. The results show that the computer vision method can be applied to extract unsteady CSF flow information. We also discuss observations and identify future areas for improvement by integrating CFD simulations for validation as a vital component for studying CSF dynamics.

Keywords: Time-SLIP · MRI · Cerebrospinal fluid · Computer vision

1 Introduction

Cerebrospinal fluid (CSF) is a clear, colorless fluid in the ventricles and subarachnoid space, enveloping and supporting the brain and spinal cord [1, 2]. Although the CSF system only accounts for ~10% of the entire cerebral cavity, it is pivotal in cushioning the brain within its bony enclosure, providing structural support and protection, and facilitating brain metabolism by transporting nutrients, removing metabolic waste, and maintaining chemical balance [3, 4]. CSF motion is influenced by complex interactions among head motions, arterial pulsations, and respiratory cycles [5, 6]. Naturally there remains a strong interest in understanding the CSF response to head motions, *e.g.*, those due to active exercise or to uninitiated rapid impacts (*i.e.*, a blow to the head).

H. R. Arabnia et al. (Eds.): CSCI 2024, CCIS 2511, pp. 212–225, 2025.
https://doi.org/10.1007/978-3-031-94962-3_19

Traditional CSF flow dynamics imaging studies rely on contrast media and fluorescent agents to capture motion and have proven useful in anatomy and diagnostics but cannot provide precise and comprehensive measurements of velocity or direction, unless specialized techniques like Phase-Contrast MRI are used, or resolve fast or complex fluid dynamics. For instance, 4D MRI, though effective for non-invasive visualization and quantification of CSF flow in the brain and spinal cord, is resource-intensive, requiring significant time and operational costs as well as expensive hardware and software. In addition, the interpretation of 4D flow imaging results, which requires signal averaging, can be compromised when data are collected using only cardiac gating in the presence of multiple driving forces, such as CSF flow pulsation. In contrast, Time-Spatial Labeling Inversion Pulse (Time-SLIP) MRI [7–9] offers a cost-effective alternative that can be implemented on existing MRI systems with minimal upgrades. This technique selectively labels or "inverts" the magnetization of specific regions at a chosen time, allowing for non-invasively tracking the movement of fluid over time within those regions. Time-SLIP MRI provides both high-resolution brain anatomy imaging and real-time visualization of CSF flow patterns [10], making it particularly useful for conditions like hydrocephalus or studying CSF dynamics around brain structures. Compared to 4D MRI, Time-SLIP is more affordable, practical for qualitative imaging and flow visualization, and requires less radiologist time, computational resources, and interpretation effort.

Utilizing Time-SLIP MRI to study CSF dynamics requires a robust DICOM image processing workflow and a reliable pipeline for extracting unsteady flow field information. In this study, each patient's scan generated three sets of DICOM images: one set showing brain anatomy in all three planes, another set of images recorded on the mid-sagittal and mid-axial planes in the stationary head, and a third set of images taken on the mid-sagittal plane during instructed head motion. The workflow began with SPM12 (a medical-image processing tool) [11], which was used to remove the skull from the anatomical MRI images and segment the resulting T1-weighted images to extract CSF anatomical geometry using 3D Slicer. Next, OpenCV [12] was employed to track fluid motion and estimate instantaneous velocities at discrete points of interest from the non-anatomical image sets. Subsequently, SPM12's realignment functionality was utilized on the head-motion image set to calculate the head's time-varying translational and rotational displacements and thereby generate the head-motion schedules. Finally, the CSF geometry and head-motion schedules were imported into a computational fluid dynamics (CFD) software [13], to simulate ventricular CSF flow [14], enabling comparison with the velocity estimates derived by application of the computer vision method to Time-SLIP MRI medical images.

This work is significant as it introduces a robust toolset for advancing research in CSF dynamics. It leverages Time-SLIP MRI to revisit fundamental aspects of CSF physiology and gain deeper insights into its roles in both normal and pathological states. Additionally, it facilitates the assessment of how head movement and respiration influence CSF dynamics, enhances understanding of phenomena such as contrecoup injuries, and provides critical insights into the pathological progression of concussive brain injury.

2 Methodology

2.1 Processing of DICOM Images with SPM

In the clinical setting, each subject's scan generated three sets of DICOM images: one set showing brain anatomy in all three planes (sagittal, axial, and coronal), another set capturing images on the mid-sagittal and mid-axial planes while the head was stationary, and a third set consisting of images taken on the mid-sagittal plane during instructed head motion. The last two sets are Time-SLIP MRI images that show the CSF flow. The anatomy set contained both T1- and T2-weighted images. In T1-weighted images, tissues with shorter T1 relaxation times, like adipose tissue, appear hyperintense (bright), while those with longer T1 times, such as CSF, appear hypointense (dark). As a result, CSF appears darker, while cortical tissue displays a lighter gray-white contrast.

To minimize noise from the skull in brain MRI images and accurately evaluate CSF volumes, the images were pre-processed using the Statistical Parametric Mapping (SPM) tool. SPM12, a comprehensive MRI research software, offers built-in toolboxes for noise reduction, preprocessing, registration, batch processing, and statistical analysis [11]. In this study, preprocessing was performed with T1-weighted imaging using the Computational Anatomy Toolbox (CAT) within SPM, selecting the Eastern Asian template to account for the anatomical characteristics of Japanese population. The Eastern Asian template, designed for populations with a higher cranial vault accommodating a larger brain, ensures greater accuracy in image analysis. The CAT toolbox leverages deep learning algorithms for automatic segmentation, effectively identifying anatomical structures such as brain ventricles, white matter (WM), gray matter (GM), and skull. Figure 1 illustrates the spatial distribution and composition of brain tissues before and after segmentation, which was performed using a probabilistic atlas and a Gaussian Mixture Model (GMM) approach. This approach enabled the conversion of MRI images into T1- and T2-weighted formats while effectively removing skull artifacts. In the right panel below, the red regions represent white matter, while the blue regions correspond to the skull, as segmented by CAT. Time-SLIP MRI makes it possible to visualize CSF dynamics. In this study, key parameters for our images include: 1.2-mm slice thickness, 0.6-mm spacing between slices, 96 encoding steps, 123.2-Hz imaging frequency, and 196 echo train length.

2.2 Geometric Construction of CSF Anatomy

3D Slicer was employed to process SPM-generated NIfTI files and accurately construct 3D models from the processed T1-weighted images. Preprocessing DICOM images in SPM12 before importing them into 3D Slicer for anatomy provides several key advantages: (1) Spatial Normalization: Aligns images to a standard template and enables group analyses and the use of standard atlases in 3D Slicer. (2) Segmentation: Separates tissue types for targeted CSF analysis within 3D Slicer. (3) Bias Field Correction: Mitigates intensity inhomogeneities caused by scanner imperfections and ensures consistent image quality. (4) Realignment: Addresses motion artifacts in longitudinal or multi-slice scans, which may not be as effectively handled by 3D Slicer. (5) Co-registration: Ensures precise alignment of multi-modal datasets (*e.g.*, T1-weighted, T2-weighted, or *f*MRI)

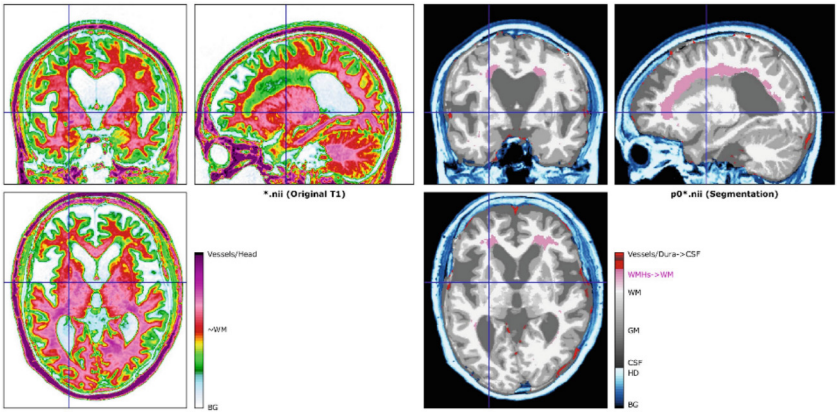

Fig. 1. Color-coded representation of brain structures before (left) and after (right) segmentation

before importing them into 3D Slicer for further processing, such as segmentation or surgical planning.

3D Slicer [15], an open-source medical segmentation tool, facilitates the segmentation of raw images and the construction of 3D models using manual and semi-automatic methods. To create and evaluate the accuracy of a 3D ventricle model, two approaches were compared: manual frame-by-frame modeling and semi-automatic seed modeling. In the manual method, MRI images were analyzed frame by frame using the "level tracing" function to outline the approximate CSF contours in each plane, followed by refinements with the "painting" tool. Finally, the model was smoothed using the "Median Smoothing" method with a 1.60-mm kernel size to enhance precision. Figure 2 illustrates the green-highlighted ventricle structure across different levels.

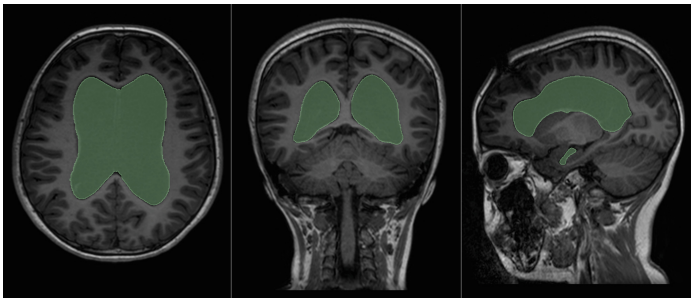

Fig. 2. The level-tracing and painting procedure for the construction of the ventricular CSF space

By repeating this process, a complete and accurate model was constructed. n the semi-automatic bubble approach, the "seed" function was employed to define both the starting point and the boundary. This function in 3D Slicer operates based on the Grow-Cut Algorithm, which uses an iterative labeling process. User-defined "seed" pixels propagate to neighboring pixels according to local transition rules. These rules rely on

image features such as intensity differences and neighborhood relationships to determine propagation. Propagation is influenced by the similarity between a pixel and its neighbors, where more similar pixels exert a stronger influence. Each pixel updates its label and confidence level by evaluating the influence of its neighboring pixels, prioritizing the strongest label influence. The process iteratively updates labels and confidence values until no further changes occur, ensuring stable and accurate segmentation [16]. This approach balances local competition and global coherence, allowing user-defined seeds to guide the segmentation effectively.

In Fig. 3, green labeling marks led to the green-highlighted ventricle structure, while yellow labeling marks yielded its boundary. The automatically generated model was trimmed and then refined using the "Joint Smoothing" method with a 50% smoothing factor. To ensure accuracy, the model was compared to the original MRI scans, verifying that it accurately reflected the anatomical structure. In 3D Slicer, 3D objects can be smoothed globally using two methods: median smoothing, which removes small extrusions and fills gaps while preserving smooth contours, and joint smoothing, which smooths multiple segments simultaneously while maintaining watertight interfaces between them. Based on our experience, joint smoothing is preferred when using the semi-automatic bubble approach.

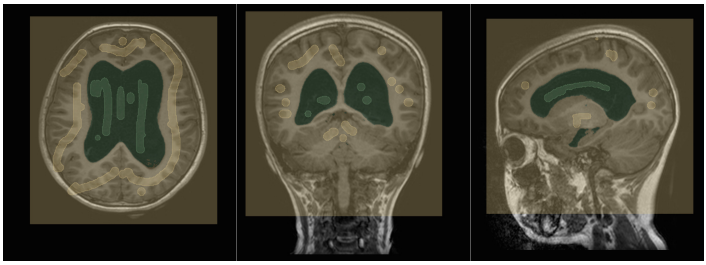

Fig. 3. The seeding-and-bubbling procedure for the construction of the ventricular CSF space

2.3 Fluid Motion and Velocity Estimation

In this study, each subject's comprehensive scan generated three sets of images: one brain-anatomy set, another set capturing CSF flow movement on the mid-sagittal and mid-axial planes under stationary head conditions, and a third set capturing CSF flow movement on the mid-sagittal plane during instructed head motion. To study CSF flow and the effects of factors such as head motion, arterial pulsations, and respiratory cycles, the Time-SLIP (*i.e.*, non-anatomy) images in 140-ms intervals were compiled into video clips to track flow paths in regions like the third ventricle and estimate velocity distribution. Each video was analyzed using the optical flow method from the OpenCV library, which calculates motion by tracking pixel movement. This method assumes constant brightness over short intervals and similar motion patterns among adjacent pixels, generating optical flow vectors that represent velocity and direction. The Farneback algorithm, used for this analysis, models local image regions with quadratic polynomials

and tracks changes between consecutive frames to estimate motion. In the Farneback algorithm, the motion of each pixel between two adjacent frames is modeled using an expanded Taylor series [17]. Known for its efficiency and precision, this dense optical flow method effectively captures subtle motion variations, making it well-suited for analyzing CSF flow in the third and fourth ventricles.

Before analyzing CSF flow with the Farneback optical flow algorithm, the images were preprocessed using a Gaussian filter for smoothing and a multi-scale pyramid for scalability. Smoothing reduced noise while preserving image quality by fine-tuning the filter strength. The image pyramid, created by progressively down-sampling the image (typically halving its dimensions at each level), allowed the algorithm to detect large-scale movements at lower resolutions and refine small-scale details at higher resolutions. Figure 4 illustrates how velocity was determined at six specific points across MRI images taken at different times. While a dense grid could estimate velocity at all points, only regions near the magnetization inversion (marked by three zones in each image) produced reliable results. Thus, as shown in Fig. 4, velocity was estimated only at discrete points: four in the third ventricle, one at the aqueduct's upper end, and one in the fourth ventricle, focusing on the flow area of interest. Note that the three bright vertical stripes in Fig. 4 represent the areas where proton magnetization was inverted in Time-SLIP imaging.

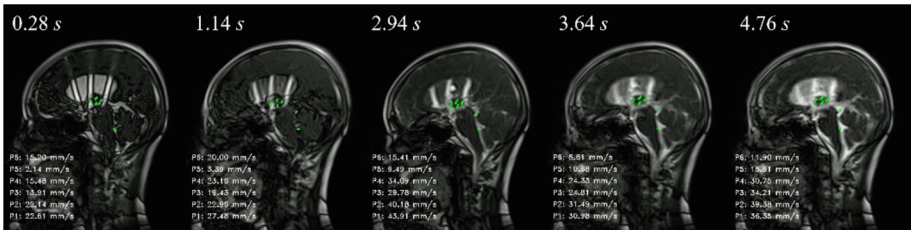

Fig. 4. Velocity estimation for six probe points at five instants of time

2.4 Extraction of Head-Motion Schedules

The 3D geometry of the ventricular CSF space was imported to a CFD software package [13] to simulate the unsteady CSF flow field and study its flow dynamics. This work had two primary objectives. First, vortex formation was observed in the third ventricle from Time-SLIP MRI and should be validated by CFD. Second, CFD simulations assist in examining how head movements affect the CSF flow by simulating movements beyond those prescribed by clinicians. To validate the simulation setup, CSF flow predictions, including velocity at various probe points, were compared with OpenCV analysis of Time-SLIP images. Motion schedules extracted from Time-SLIP images recorded during guided head movements were used as inputs for the moving-head simulation.

To extract the head-motion schedules, the re-align function in SPM was utilized. The first DICOM image served as the reference to compare skull positions across subsequent images in the same scan sequence. Temporal head movements were initially expressed as translational and rotational displacements, which were then converted into instantaneous

centers of rotation and rotational speeds for CFD simulations. The accuracy of the alignment was confirmed by applying the calculated displacements to revert each skull position back to the original reference image. Figure 5 illustrates the confirmation process across five time points, with each column representing a specific moment. The bottom row displays the reference image, while the top two rows show pre-alignment and post-alignment images, respectively. The alignment's accuracy is validated by the coincidence of the skull position in the post-alignment images (middle row) with the original position in the reference images (bottom row).

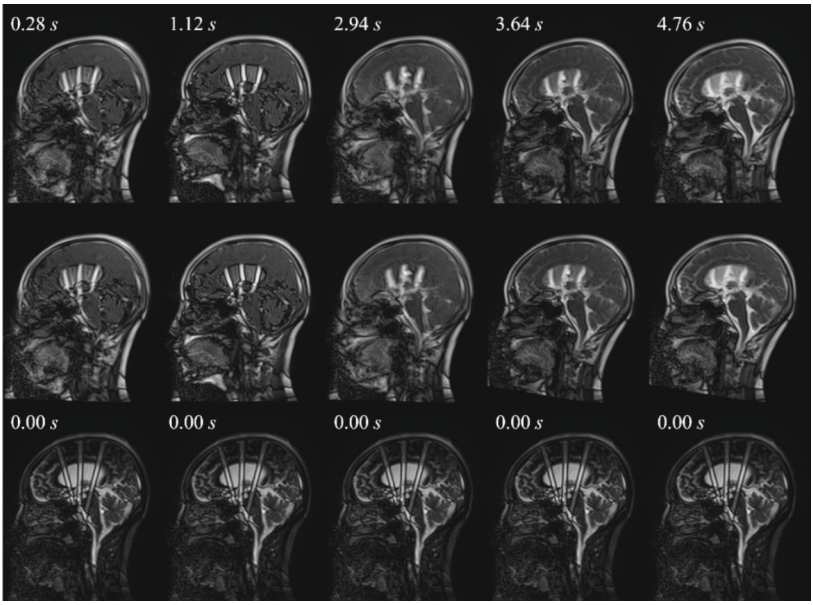

Fig. 5. Images at five different instants (in columns), before (top row) and after (middle row) the realignment based on the reference image (bottom row)

3 Validation and Results

Our image processing workflow began with SPM12, which handled skull removal, generated segmentation outputs (*e.g.*, CSF volume), and produced T1-weighted images for further refinement in 3D Slicer. For example, one subject's CSF volume was calculated as 446 cm^3, accounting for 29.4% of the brain. These results were validated using *SolidWorks*, a CAD modeling software [18]. In SPM12, the determination of the margin at the skull base subarachnoid space during brain MRI preprocessing relies on tissue probability maps (TPMs), bias correction, and spatial regularization. (1) TPMs for gray matter, white matter, CSF, and non-brain tissues, aligned with a standard anatomical template (*e.g.*, MNI space), guide the segmentation process, with the CSF TPM specifically covering the subarachnoid space and ventricles. (2) Bias field correction mitigates

intensity inhomogeneities, particularly at the skull base, ensuring consistent voxel intensities for accurate CSF space classification. The segmentation algorithm combines voxel intensities, probabilistic priors from the TPMs, and spatial constraints to delineate tissue boundaries, including the skull base subarachnoid space. (3) Spatial regularization smooths the segmentation to avoid abrupt changes in tissue classification, while normalization to standard space aligns the subject's anatomy with template priors. However, the accuracy of margin delineation depends on MRI resolution, contrast between tissues, and alignment with the TPMs. In cases of pathology or anatomical variation, manual adjustments or high-resolution scans may be necessary for precise delineation.

SPM12-generated NIfTI files were processed in 3D Slicer using either a manual or semi-automatic method to construct accurate 3D models from the T1-weighted images. Figure 6 illustrates the 3D ventricle model of a subject with hydrocephalus, with the dark background highlighting the segmentation process. The CSF ventricular geometry (rendered in gold) was further analyzed with *SolidWorks* and compared, slice by slice, with the original MRI images, confirming its conformity to the actual anatomy.

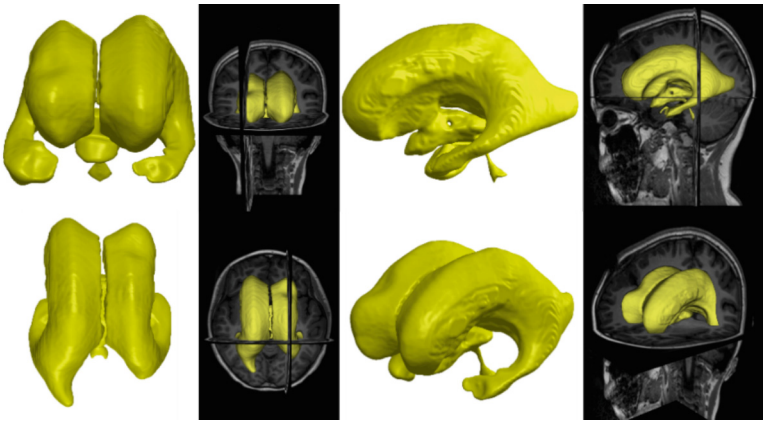

Fig. 6. A ventricle model obtained through 3D Slicer segmentation

Subsequently, the 3D ventricle model was imported into the CFD solver to simulate the CSF flow under both stationary-head and moving-head conditions. To compare the CFD simulations with image processing results, Time-SLIP images recorded both under stationary-head conditions and during guided head movements were processed with OpenCV to obtain the corresponding CSF flow field. Figure 7 demonstrates the CSF flow computational model of a subject rendered in CFD simulations and discretized into computational mesh cells. The meshes are shown on the mid-sagittal section and the CSF surface. For each subject's large eddy simulation (LES) of CSF flow, a mesh sensitivity study was performed to ensure a balance between simulation accuracy and convergence. The key parameters in the simulation set-up included a 0.16-mm base size, 8 prism layers, and a volume growth rate of 1.1. This configuration resulted in a cell count of approximately 6–8 million, depending on the size of the subject's ventricles.

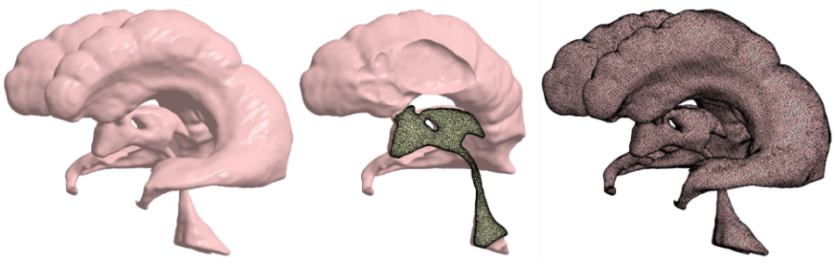

(a) (b) (c)

Fig. 7. (a) Ventricle geometry of a subject imported for CFD simulation, (b) CFD volume meshes shown on the mid-sagittal section, (c) CFD surface meshes shown on the surface of the ventricle geometry

The simulation used the implicit SIMPLE solver with 30 inner iterations per time step of 0.1 ms. Three cylindrical pipes, each with an inner diameter of 6 mm, were connected to the bottom and sides of the fourth ventricle to serve as input and output, respectively. For the input boundary, a mass flow rate was specified with a 1 *Hz* oscillation corresponding to the cardiac frequency (60 bpm resting heart rate) and additional disturbances represented by higher harmonics at 2 Hz and 11.85 Hz. In the moving-head simulation, head motion was not activated until 4 s, allowing the CSF flow to fully develop across the computational domain and giving simulation sufficient time to reach statistically steady state. Typically, during a Time-SLIP MRI sequence, the head motion lasted for 9.66 s, corresponding to the 4–13.66 s interval in the simulation, which generally concluded at 30 s. Figure 8a illustrates the head motion schedule for one case, where a positive rotation angle indicates nose-down motion. An FFT (Fast Fourier Transform) analysis of the rotational speed produced a single-sided amplitude spectrum (Fig. 8b), revealing that the doctor-guided head motion occurred at an approximate frequency of 2 Hz in this case.

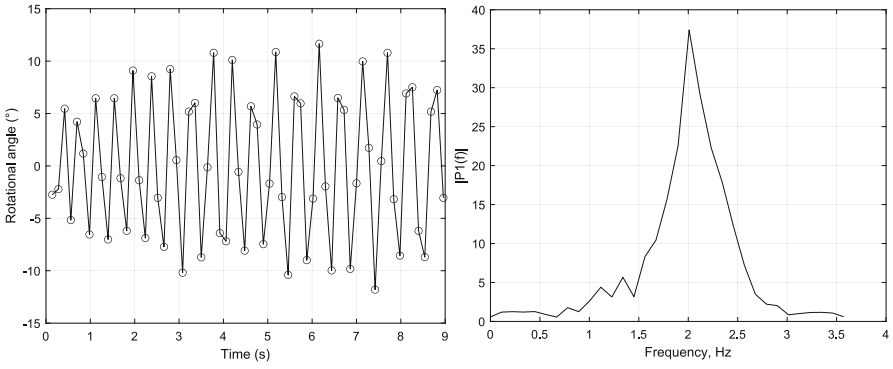

(a) (b)

Fig. 8. (a) Temporal rotational angle determined from a set of Time-SLIP images, (b) FFT spectrum for the corresponding rotational speed

4 Discussion and Conclusions

Sophisticated imaging techniques are essential for CSF dynamics research, providing detailed insights into CSF movement in response to physiological processes like the cardiac cycle and respiratory motion. Time-SLIP dynamically visualizes CSF flow by applying an RF pulse to invert proton magnetization in a selected region, *e.g.*, the three vertical zones in Fig. 4 and the horizontal zone in Fig. 9a. After a controlled delay, during which the labeled fluid moves, images are acquired to track its flow through associated structures over time. This process is repeated with varying delays to create a detailed visualization of fluid dynamics. Using OpenCV, we analyzed Time-SLIP images to track pixel changes between consecutive frames and estimate motion at specific locations. The process relies on the Farneback algorithm, which generates optical flow vectors representing velocity and direction.

As illustrated in Fig. 9a, six representative points within each subject's CSF ventricles were selected to measure velocity: four in the third ventricle—anterior (pt. #1), superior (pt. #2), posterior (pt. #3), and inferior (pt. #4)—one (pt. #5) at the aqueduct's upper end, and one (pt. #6) in the fourth ventricle. Note that the results in Fig. 9 belong to a different subject from Figs. 4 and 5. The right panel in Fig. 9a shows the corresponding locations in the CFD simulation setup. Figure 9b depicts the running-average velocity profiles at these points during a moving-head scan. Ideally, the initial velocity should be zero since no reference image is available for comparison. However, a finite value is used because of the running average operation. From the stabilized portion of the velocity profiles, shown in Fig. 9b to begin around 3 s, the average velocities at the six locations were estimated as 13.6 mm/s, 25.6 mm/s, 32.5 mm/s, 22.1 mm/s, 51.9 mm/s, and 72.9 mm/s, respectively.

FFT analysis was conducted on the fluctuating velocity for each case to identify the frequency content in the velocity signals. Overall, the frequency contents of the six velocities showed good agreement. Nonetheless, pts. #3 and #5 provided more reliable results because of their closer proximity to the magnetization labeling zone in Time-SLIP imaging and the direct influence of CSF influx from the aqueduct. Thus, Fig. 9c focuses on the single-sided amplitude spectra for these two locations, including their CFD counterparts for comparison. All spectra have been normalized to their respective max values. As expected, the solid lines in Fig. 9c reveal two predominant harmonics: the subject's resting heart rate (1–1.6 Hz) during the MRI scan and the doctor's motion guidance frequency (~2 Hz, as shown in Fig. 8). Other modes correspond to peak frequencies associated with critical CSF geometries, such as the sharp tapering from the fourth ventricle to the aqueduct neck and the shape and size of the *massa intermedia*. Higher harmonics likely result from interactions between these lower harmonics.

Each CFD simulation of CSF flow consisted of a 4-s stationary phase, a 9.66-s motion phase, and a final 16-s stationary phase, with FFT analysis performed on the resulting fluctuating velocity data. Figure 10 was generated using the CSF geometry from Figs. 7 and 9a and the motion schedule from Fig. 8. It aligns with Fig. 9 by focusing exclusively on the 9.66-s motion phase results. Figures 9b and 10 indicate that both the CFD-predicted velocity profiles and MRI velocity estimates fall within the range of 10–110 mm/s, with points #1 and #4 exhibiting the closest agreement in magnitude. From

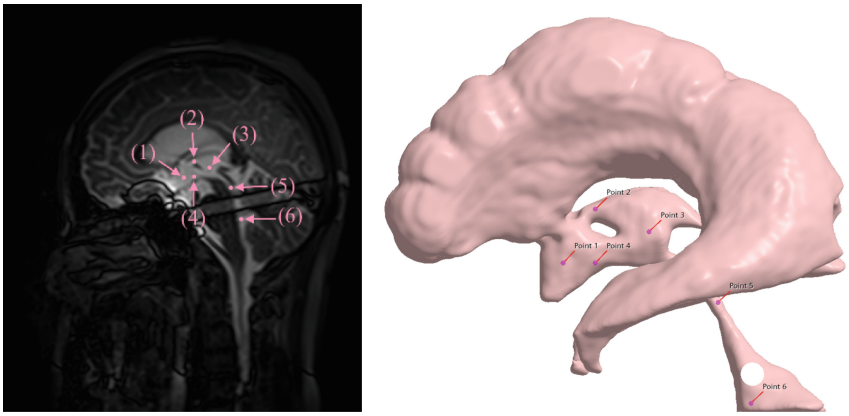

(a)

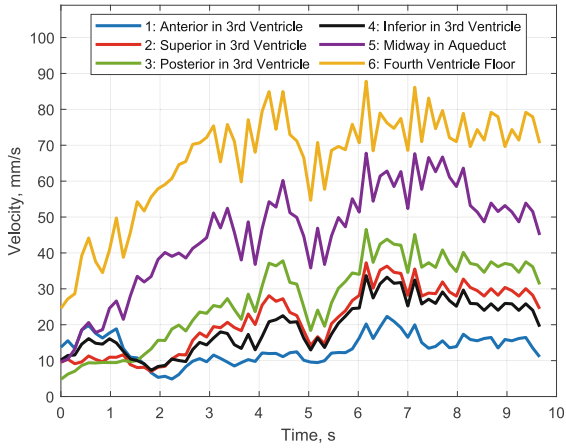

(b)

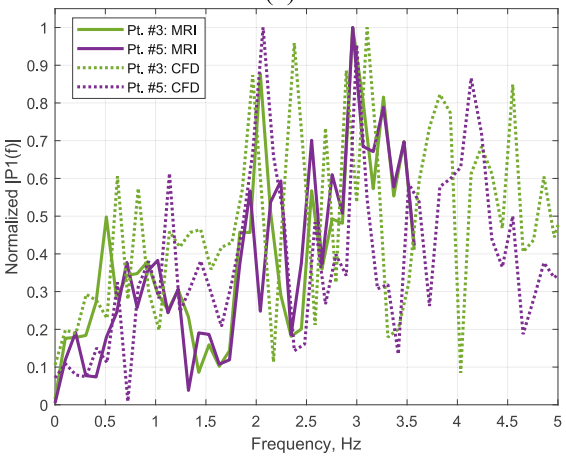

(c)

Fig. 9. (a) Locations of the six representative probe points in the ventricular CSF space, (b) MRI-deduced velocities at the six representative probe points, (c) FFT spectra at two probe points

the CFD velocity predictions, the average velocities at the six locations were estimated as 13.7 mm/s, 14.6 mm/s, 15.6 mm/s, 17.3 mm/s, 79.1 mm/s, and 29.9 mm/s, respectively.

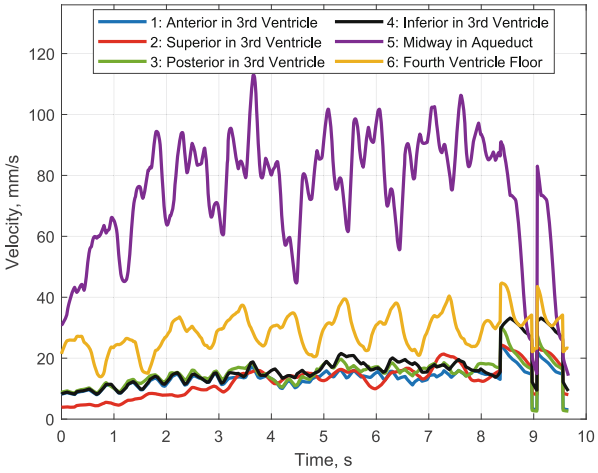

Fig. 10. CFD-deduced velocities at the same six probe points as in Fig. 9

As expected, discrepancies exist between the CFD-predicted and OpenCV-estimated velocity profiles, likely due to several contributing factors. First, OpenCV's assumptions—such as constant brightness over short intervals and consistent motion patterns between adjacent pixels—are not always valid in the MRI image sequence that was used for this study. Although achieving high spatial and temporal resolution simultaneously can be challenging, the acquisition time (*i.e.*, 0.14-s interval between frames) may be too long to accurately estimate velocity vectors. Second, the subject's head motion likely deviated from the mid-sagittal plane, meaning the motion schedule extracted from MRI images and used as input for CFD simulations may be inaccurate. Lastly, some reference points, such as point #6, might have shifted out of the Time-SLIP MRI scan plane or field of view, leading to uncertain velocity estimates.

Figure 9c presents the CFD-derived FFT spectra (dotted lines) for pts. #3 (highlighted in green) and #5 (purple). As expected, the CFD results capture a 1-Hz harmonic corresponding to the prescribed 60-bpm cardiac frequency, as well as a 2-Hz harmonic associated with the frequency of the subject's head motion. The FFT spectra also reveal that the CSF flow velocity fluctuations contain fluctuation modes of other frequencies. Notably, the CFD spectra extend to higher frequencies due to their better temporal resolution (0.01-s intervals in CFD compared to Time-SLIP's 0.14-s intervals). This highlights the need for improved temporal resolution in Time-SLIP MRI imaging.

Locations such as points #1, #2, and #4—farther from the proton magnetization inversion in Time-SLIP imaging or the direct influence of CSF influx from the aqueduct—tend to yield less reliable flow-speed results compared to closer locations. This underscores the advantages of using multiple Time-SLIP labeling zones, as shown in scans of another subject (Fig. 5), and expanding the proton magnetization inversion area for studying CSF flow. However, Time-SLIP MRI imaging is zonal and cannot

encompass the entire CSF region. Therefore, CFD simulations are essential for complementing Time-SLIP imaging, as they provide otherwise unavailable flow-field data, including velocities and pressures, in regions beyond the reach of Time-SLIP labeling.

Acknowledgements. This material is based upon work supported by the National Science Foundation of the United States of America under Grant No. 2232598. The first author also has been supported by the Science & Technology Department of Sichuan Province Award (No. 2023NSFSC0058), while working at Sichuan University-Pittsburgh Institute. We acknowledge SPM12 (GNU General Public License) for its comprehensive tools in brain imaging analysis, OpenCV (Apache 2.0 License) for its robust image processing capabilities, and 3D Slicer (BSD-style license) for its powerful 3D biomedical image visualization.

References

1. Weed, L.H.: Studies on cerebro-spinal fluid. No. IV: the dual source of cerebro-spinal fluid. J. Med. Res. **31**(1), 93–118 (1914)
2. Weed, L.H.: Studies on cerebro-spinal fluid. No. III: the pathways of escape from the subarachnoid spaces with particular reference to the arachnoid villi. J. Med. Res. **31**(1), 51–91 (1914)
3. Weed, L.H.: Studies on cerebro-spinal fluid. No. II: the theories of drainage of cerebro-spinal fluid with an analysis of the methods of investigation. J. Med. Res. **31**(1), 21–49 (1914)
4. Cushing, H.: Studies on the Cerebro-Spinal Fluid: I. Introduction. J. Med. Res. **31**(1), 1–19 (1914)
5. Yamada, S., et al.: Influence of respiration on cerebrospinal fluid movement using magnetic resonance spin labeling. Fluids Bar. CNS **10**(1), 36 (2013)
6. Martin, B.A., Loth, F.: The influence of coughing on cerebrospinal fluid pressure in an *in vitro* syringomyelia model with spinal subarachnoid space stenosis. Cerebrospinal Fluid Res. **6**, 17 (2009)
7. Yamada, S.: Cerebrospinal fluid dynamics. Croat. Med. J. **62**(4), 399–410 (2021)
8. Yamada, S.: Cerebrospinal fluid physiology: visualization of cerebrospinal fluid dynamics using the magnetic resonance imaging time-spatial inversion pulse method. Croat. Med. J. **55**, 337–346 (2014)
9. Shiodera, T., Nitta, S., Takeguchi, T., et al.: Automated flow quantification for spin labeling MR imaging. Magn. Reson. Mater. Phy. **27**(5), 425–433 (2014)
10. Yamada, S.: Use of a spin-labeled cerebrospinal fluid magnetic resonance imaging technique to demonstrate successful endoscopic fenestration of an enlarging symptomatic cavum septi pellucidi. World Neurosurg. **80**(3–4), 436.e15-436.e18 (2013)
11. SPM12 Users Manual. https://www.fil.ion.ucl.ac.uk/spm/doc/manual.pdf
12. Bradski, G.: The OpenCV library. Dr. Dobb's J. Softw. Tools **120**, 122–125 (2000)
13. STAR CCM+ Users Manual. https://www.plm.automation.siemens.com/global/en/products/simcenter/STAR-CCM.html
14. Liou, W. W, Yang, Y., Yamada, S.: Cerebrospinal fluid flow simulations in brain ventricles with elastic wall responses. In: 6th International Conference on Computational and Mathematical Biomedical Engineering, 10–12 June. Tohoku University, Japan (2019)
15. Fedorov, A., et al.: 3D slicer as an image computing platform for the quantitative imaging network. Magn. Reson. Imaging **30**(9), 1323–1341 (2012)
16. Thomas, H.M.: Hybrid positron emission tomography segmentation of heterogeneous lung tumors using 3D slicer: improved growcut algorithm with threshold initialization. J. Med. Imag. **4**(1), 011009 (2017)

17. Farnebäck, G.: Two-frame motion estimation based on polynomial expansion. In: Bigun, J., Gustavsson, T. (eds.) Image Analysis. SCIA 2003. LNCS, vol. 2749. Springer, Berlin, Heidelberg (2003). https://doi.org/10.1007/3-540-45103-X_50
18. Dassault Systèmes SolidWorks Corporation. SolidWorks User's Guide 2020. Dassault Systèmes, Waltham, MA (2020)